

DAY-SIDE Z'-BAND EMISSION AND ECCENTRICITY OF WASP-12B¹

MERCEDES LÓPEZ-MORALES^{2,4}, JEFFREY L. COUGHLIN^{3,5}, DAVID K. SING⁶, ADAM BURROWS⁷, DÁNIEL APAI⁸, JUSTIN C. ROGERS^{4,9} & DAVID S. SPIEGEL⁷
 e-mail: mercedes@dtm.ciw.edu

ABSTRACT

We report the detection of the eclipse of the very-hot Jupiter WASP-12b via z'-band time-series photometry obtained with the 3.5-meter ARC telescope at Apache Point Observatory. We measure a decrease in flux of $0.082 \pm 0.015\%$ during the passage of the planet behind the star. That planetary flux is equally well reproduced by atmospheric models with and without extra absorbers, and a black-body model with $T_{z'} \sim 2660\text{K}$, $A_B < 0.3$, and $P_n \sim 0.5$. The eclipse is centered at phase $\phi = 0.5100 \pm 0.0022$, consistent with an orbital eccentricity of $|ecosw| = 0.0156 \pm 0.0035$. Assuming the eccentricity is caused by other planets in the system and atmospheric opacities corresponding to solar metallicity abundance, the large radius of WASP-12b can be explained by tidal heating if $Q'_p < 3.82 \times 10^7$.

Subject headings: planetary systems — stars: individual: WASP-12 — techniques: photometric

1. INTRODUCTION

The transiting Very Hot Jupiter WASP-12b, discovered by Hebb et al. (2009), has many notable characteristics. With a mass of $1.41 \pm 0.10 M_{Jup}$ and a radius of $1.79 \pm 0.09 R_{Jup}$, WASP-12b is the planet with the second largest radius to date, only surpassed by WASP-17b (Anderson et al. 2009). It is also the most heavily irradiated planet known, with an incident stellar flux at the substellar point of over $9 \times 10^9 \text{ erg cm}^{-2} \text{ s}^{-1}$. In addition, model fits to its observed radial velocity and transit light curves suggest that the orbit of WASP-12b is slightly eccentric. All these attributes make WASP-12b one of the best targets to test current irradiated atmosphere and tidal heating models for extrasolar planets.

In irradiated atmosphere model studies WASP-12b is an extreme case at the top of the category of highly irradiated hot planets. Such highly irradiated planets are expected to show thermal inversions in their upper atmospheric layers (Burrows et al. 2008), although what chemicals are responsible for such thermal inversions remains unknown. TiO and VO molecules, which can act as strong optical absorbers, have been proposed (Hubeny et al. 2003; Fortney et al. 2008), but Désert et al. (2008) claim that the concentration of those molecules in planetary atmospheres is too low ($< 10^{-3} - 10^{-2}$ times solar). Spiegel et al. (2009) argue that TiO

needs to be at least half the solar abundance to cause thermal inversions, and very high levels of macroscopic mixing are required to keep enough TiO in the upper atmosphere of planets. S_2 , S_3 and HS compounds have also recently been suggested first and then questioned as causes of the observed thermal inversions (Zahnle et al. 2009a,b).

In the case of tidal heating, detailed models are now being developed (e.g. Bodenheimer et al. 2003; Miller et al. 2009; Ibgui et al. 2009,b; Ibgui & Burrows 2009) to explain the inflated radius phenomenon observed in hot Jupiters, of which WASP-12b, with a radius 40% larger than predicted by standard models, is also an extreme case. All models assume that the planetary orbits are slightly eccentric, and directly measuring those eccentricities is key not only to test the model hypotheses, but also to obtain information about the planets' core mass and energy dissipation mechanisms (see e.g. Ibgui et al. 2009).

Here we present the detection of the eclipse of WASP-12b in the z'-band ($0.9 \mu\text{m}$), which gives the first measurement of the atmospheric emission of the planet, and the first direct determination of its orbital eccentricity. Section 2 summarizes the observations and the analysis of the data. In Sections 3 and 4 we discuss the tidal dissipation factor of the planet and compare its emission to models. The results are discussed in Section 5.

2. OBSERVATIONS AND ANALYSES

We monitored WASP-12 [RA(J2000) = 06:30:32.794, Dec(J2000) = +29:40:20.29, V=11.7] during two eclipses on February 19 and October 18 2009 UT, both nights photometric, with an additional attempt on October 30 2009 UT lost due to weather. We used the SPICam instrument on the ARC's 3.5-meter telescope at Apache Point Observatory with a SDSS z' filter, which when convolved with the wavelength response curve of the SPICam CCD yields an effective central wavelength of $\sim 0.9 \mu\text{m}$. SPICam is a backside-illuminated SITE TK2048E 2048x2048 pixel CCD with 24 micron pixels, giving an unbinned plate scale of 0.14 arc seconds per pixel and a field of view of 4.78 arc minutes square. The detector, cosmetically excellent and linear through the full A/D

¹ Based on observations collected with the Apache Point Observatory 3.5-meter telescope, which is owned and operated by the Astrophysical Research Consortium (ARC).

² Hubble Fellow

³ NSF Graduate Research Fellow

⁴ Carnegie Institution of Washington, Department of Terrestrial Magnetism, 5241 Broad Branch Rd. NW, Washington D.C., 20015, USA

⁵ Department of Astronomy, New Mexico State University, Las Cruces, NM 88003, USA

⁶ Astrophysics group, School of Physics, University of Exeter, Stocker Road, Exeter, Ex4 4QL, United Kingdom

⁷ Princeton University, Department of Astrophysical Sciences, Peyton Hall, Princeton, NJ, 08544, USA

⁸ Space Telescope Science Institute, 3700 San Martin Drive, Baltimore, MD 21218, USA

⁹ Johns Hopkins University, Department of Physics and Astronomy, 366 Bloomberg Center, 3400 N. Charles Street, Baltimore, MD 21218, USA

converter range, was used with 2x2 binning, which gives a gain of $3.35 \text{ e}^-/\text{ADU}$, a read noise of 1.9 DN/pixel , and a 48 second read time.

On February 19 we monitored WASP-12 from 3:00 to 3:28 UT and from 3:54 to 7:10 UT, losing coverage between 3:28 and 3:54 UT when the star reached a local altitude greater than 85° , the soft limit of the telescope at that time. These observations yielded 1.20 hours of out-of-eclipse and 2.45 hours of in-eclipse coverage. On October 18 we extended the altitude soft limit of the telescope to 87° and covered the entirety of the eclipse from 7:05 to 12:45 UT, yielding 2.73 hours of out-of-eclipse and 2.93 hours of in-eclipse coverage. We defocused the telescope to a FWHM of $\sim 2''$ to reduce pixel sensitivity variation effects, and also to allow for longer integration times, which minimized scintillation noise and optimized the duty cycle of the observations, given the long readout times. Integration times ranged from 10 to 20 seconds. Taking into account Poisson, readout and scintillation noise, we achieved precisions on WASP-12 and other bright stars in the images of 0.8–1.6 mmag per exposure on February 19, and 0.5–1.0 mmag per exposure on October 18.

The field of view of SPICam includes WASP-12 and two other isolated stars with apparent brightness and $B - V$ and $J - K$ colors similar to the target, which minimizes differential extinction effects and makes them suitable photometric comparisons. Each night’s dataset was analyzed independently and the results combined in the end. The timing information was extracted from the headers of the images and converted into Heliocentric Julian Days using the IRAF task *setjd*, which has been tested to provide sub-second timing accuracy.

We first corrected each image from bias-level and flat-field effects using standard IRAF routines. Dark current was negligible. DAOPHOT-type aperture photometry was performed in each frame. We recorded the flux from the target and the comparison stars over a wide range of apertures and sky background annuli around each star. We used apertures between 2 and 35 pixels in one pixel steps during a first preliminary photometry pass, and 0.05 pixel steps in the final photometric extraction. To compute the sky background around each star we used variable width annuli, with inner radii between 35 and 60 pixels sampled in one-pixel steps.

The best aperture and sky annuli combinations were selected by identifying the most stable (i.e. minimum standard deviation), differential light curves between each comparison and the target. In the February 19 data, the best photometry results from an aperture radius of 14.7 pixels for both the target and the comparison stars, and sky annuli with an inner radius of 52 pixels and 22 pixel wide. For the October 18 data, 17.9 pixel apertures and sky annuli with a 45 pixel inner radius and 22 pixel wide produce the best photometry.

The differential light curves between the target and each comparison star contain systematics trends that can be attributed to either atmospheric effects, such as airmass, seeing or sky brightness variations, or to instrumental effects, such as small changes in the location of the stars on the detector. Systematics can also be introduced by instrumental temperature or pressure changes, but those parameters are not monitored in SPICam. We model systematics for each light curve by fit-

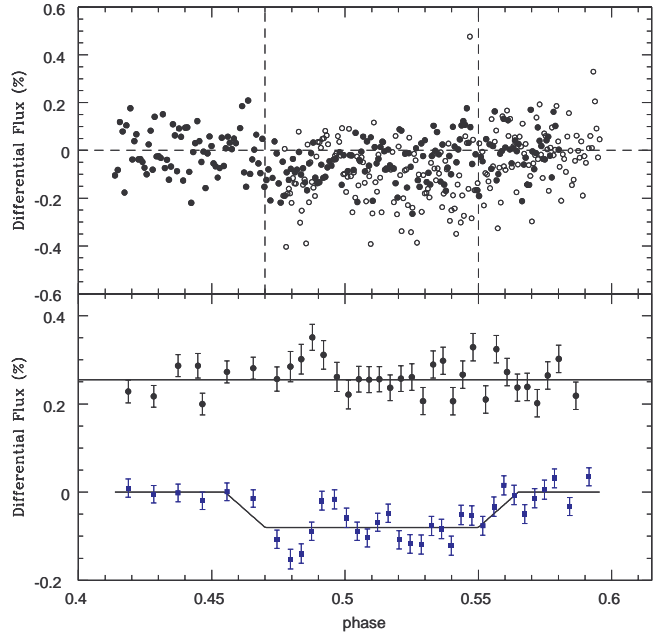


FIG. 1.— *Top*: De-trended differential light curves. Open and filled dots show, respectively, the Feb 19 and Oct 18 UT 2009 data. *Bottom*: Combined light curves binned by a factor of 12. Blue squares correspond to WASP-12 and black dots to the differential light curve of the two comparison stars. The best fit models are shown as solid lines. We attribute the flux jumps between phases 0.475 and 0.5 to unremoved systematics. Notice that, although the systematics appear in both curves around approximately the same phases, the trends in each curve are not correlated.

ting linear correlations between each parameter and the out-of-eclipse portions of the light curves. The full light curves are then de-trended using those correlation fits. In the October 18 dataset, airmass effects are the dominant systematic. The February 19 dataset also presents clear systematics with airmass, and with seeing. The systematics on this night were modeled using only the after-eclipse portion of the light curves. The pre-ingress images, i.e. 18 frames collected between 3:00 and 3:38 UT, suffer from a ~ 50 pixel position shift with respect to the rest of the images collected that night, which cannot be modeled using overall out-of-eclipse systematics. We chose not to use those points in the remaining of the analysis. Correlations with the other parameters listed above are not significant in any of the two datasets.

Finally, we produce one light curve per night by combining the de-trended light curves of each comparison. The light curves are combined applying a weighted average based on the Poisson noise of the individual light curve points. The result is illustrated in Figure 1. The out-of-eclipse scatter of the combined light curves is 0.11% for the February 19 data and 0.09% for the October 18 data. De-trending significantly improves the systematics, but some unidentified residual noise sources remain, that we have not been able to fully model.

2.1. Eclipse detection and error estimation

The two-night combined light curve contains 421 points between phases 0.413 and 0.596, based on the Hebb et al. (2009) ephemerides. To establish the presence of the eclipse and its parameters we fit the data

to a grid of models generated using the Mandel & Agol (2002) algorithm. The models include no limb darkening and use as input parameters the orbital period and the stellar and planetary radii of the system derived by Hebb et al. (2009). The best fit model is found by χ^2 minimization, with the depth, the central phase of the eclipse, and the out-of-eclipse differential flux as free parameters. The result is the detection of an eclipse with a depth of $0.082 \pm 0.015\%$ and centered at orbital phase $\phi = 0.5100 \pm 0.0022$, as shown in Figure 1. The reduced χ^2 of the fit is 0.952. The error in the eclipse depth is computed using the equation $\sigma_{depth}^2 = \sigma_w^2/N + \sigma_r^2$, where σ_w is the scatter per out-of-eclipse data point and σ_r^2 describes the red noise. The σ_r is estimated with the *prayer-bead* method (Gillon et al. 2007; Southworth 2008) and the binning technique by Pont et al. (2006) to be 1.5×10^{-4} . The prayer-bead method was also used to estimate the error in the central phase, with the result shown in Figure 3.

We investigate to what extent the uncertainties in the system's parameters affect our eclipse depth and central phase results. Varying the impact parameter, planet-to-star ratio, and scale of the system by 1σ of the reported values in Hebb et al. (2009), the measured eclipse depth changes only by 0.004% or $0.27\sigma_{depth}$, while the central phase remains unchanged. Our result is therefore largely independent of the adopted system parameters.

Finally, we performed three other tests to confirm the eclipse detection in a manner similar to previously reported eclipse results (Deming et al. 2005; Sing & López-Morales 2009; Rogers et al. 2009). Taking the average of the 125 out-of-eclipse light curve data points versus the 228 in-eclipse points (only points near the bottom of the eclipse), having adopted as central eclipse phase the value $\phi = 0.51$ obtained above, we measure an eclipse depth of $0.080 \pm 0.015\%$. We further

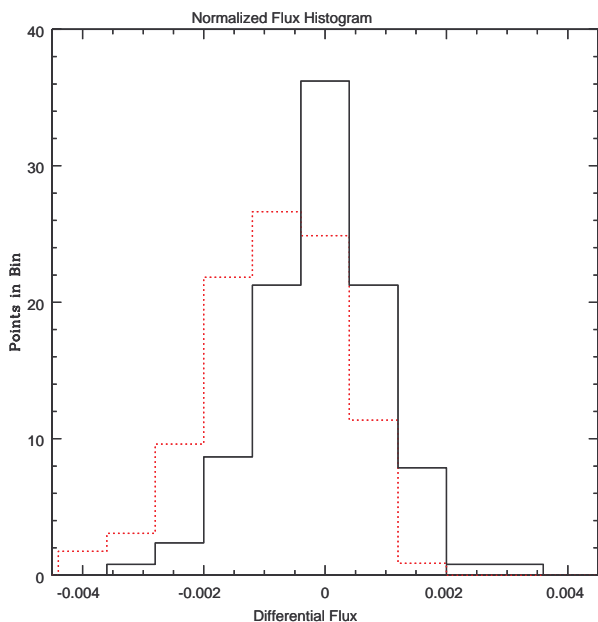


FIG. 2.— Normalized flux histograms of the in-eclipse (dotted red line) and out-of-eclipse (solid line) portions of the WASP-12 light curve in Figure 1. The bin width is 0.00082 in differential flux, coincident with the detected eclipse depth.

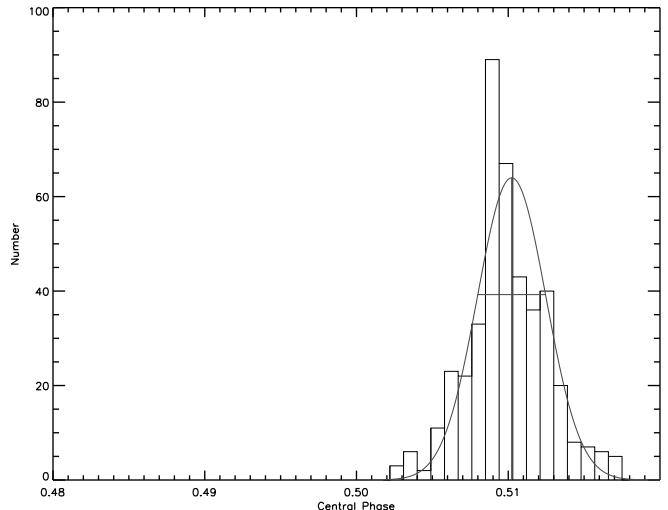


FIG. 3.— The eclipse's central phase distribution histogram resulting from the a prayer-bead analysis of the data. The distribution is well fitted by a Gaussian centered at phase $\phi = 0.51$ and with an FWHM of $\Delta\phi = 0.0022$.

check the detection by producing histograms of the normalized light curve flux distribution in the in-eclipse and out-of-eclipse portions of the light curve. The result, illustrated in Figure 3, shows how the flux distribution of in-eclipse points is shifted by 0.00082 with respect to the out-of-eclipse flux distribution, centered at zero. The results of the last test are shown in Figure 4, where by letting the depth and central phase of the eclipse vary, we confirm both parameters, i.e. a eclipse depth of $0.082 \pm 0.015\%$ and central phase $\phi = 0.51^{+0.004}_{-0.003}$. Notice that the 1σ error for the central phase in this case are larger than the one calculated using the prayer-bead method in Figure 2.

3. THE TIDAL DISSIPATION FACTOR Q'_P

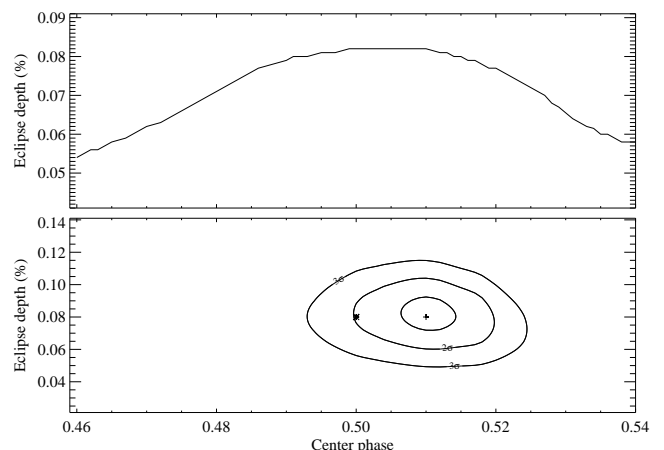


FIG. 4.— *Top*: model eclipse depth versus central phase. The x-axis scale covers the full eclipse duration. *Bottom*: Best fit model, indicated by the cross symbol at $\phi=0.51$ and depth = 0.082%, and 68.3%, 95.5% and 99.7% joint confidence contours. The star symbol at $\phi=0.50$ corresponds to a circular orbit. From the top diagram, the central phase of the eclipse is not constrained between 0.499 and 0.510, where the depths are all 0.082%. The model eclipse depth falls off rapidly for central phases outside that range. From the bottom diagram, the best-fit central phase is $0.510^{+0.004}_{-0.003}$.

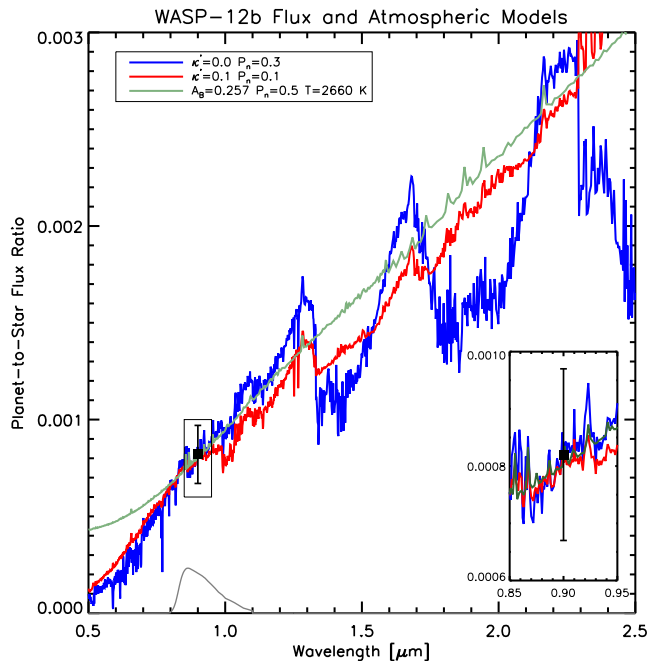


FIG. 5.— Comparison of the eclipse depth (planet-to-star flux ratio) to models. The green line shows the best fit model assuming WASP-12b emits like a black-body. The blue and red lines show, respectively, the best fit model for an atmosphere with no extra absorber, and with an extra absorber of opacity κ' between 0.43 and 1.0 μm . The black thin line at the bottom indicates the SPICam standard SDSS z' -band filter response. See Section 4 for more details.

The eccentricity e of WASP-12b was calculated from the measured central phase shift value using eq. (6) from Wallenquist (1950),

$$e \cos \omega = \frac{\pi (t_2 - t_1 - P/2)}{P (1 + \csc^2 i)}, \quad (1)$$

where P , i and ω are, respectively, the orbital period, inclination, and periastron angle of the system, and $t_2 - t_1$ is the time difference between a transit and an eclipse. In our case $t_2 - t_1 = 0.51P$. Using the values of P , i and ω obtained by Hebb et al. (2009), we derive an $e = 0.057 \pm 0.013$, which confirms the preliminary result of a non-zero eccentricity orbit for this planet reported by these authors. That eccentricity can be explained if 1) the system is too young to have already circularized, 2) there are additional bodies in the system pumping the eccentricity of WASP-12b, or 3) the tidal dissipation factor Q'_P (Goldreich 1963) of WASP-12b is several orders of magnitude larger than Jupiter's, estimated to be between 6×10^4 and 2×10^6 (Yoder & Peale 1981).

Tidal heating model scenarios where an additional planet in the system pumps the eccentricity have been proposed by Miller et al. (2009) and Ibgui et al. (2009) to explain the largely inflated radius of WASP-12b. Ibgui et al. (2009), in particular, show how different combinations of the core mass of the planet M_{core} , e , and Q'_P can lead to the same planetary radius. Using our measured eccentricity, the quotient between e and Q'_P derived by those authors in the case of planets with $M_{\text{core}} = 0$, i.e. $(e/0.05)^2 / (Q'_P/10^5)$, and the values of that quotient for WASP-12b assuming atmospheric opacities corresponding to $1\times$ and $10\times$ solar metallicity abun-

dances (see their Table 3), we conclude that Q'_P has to be $< 3.82 \times 10^7$ or $< 6.19 \times 10^8$, depending on whether the atmospheric abundance of the planet is $1\times$ or $10\times$ solar. The presence of a core would decrease the planetary radius and therefore also decrease those values of Q'_P as described in Ibgui et al. (2009).

4. COMPARISON WITH ATMOSPHERIC MODELS

We compare the observed z' -band flux of WASP-12b, first to simple blackbody models and then to expectedly more realistic radiative-convective models of irradiated planetary atmospheres in chemical equilibrium, following the same procedure described in Sect. 4 of Rogers et al. (2009). The results are shown in Figure 5.

In the blackbody case, the best fit model has a day-side brightness temperature $T_{z'} = 2660 \pm 240\text{K}$, an albedo $A_B < 0.3$, and an energy redistribution parameter $P_n \sim 0.5$. The P_n value indicates that the planet efficiently re-distributes the incident stellar irradiation throughout its atmosphere and should have uniform brightness.

The atmospheric models are derived from self-consistent coupled radiative transfer and chemical equilibrium calculations, based on the models described in Sudarsky et al. (2000, 2003), Hubeny et al. (2003) and Burrows et al. (2005, 2006, 2008). The code includes atomic and molecular opacities, irradiation from the stars using Kurucz (1993) model spectra, and heat redistribution mechanisms from the day to the night side of the planet via advection and zonal heat transport. We generate models with and without thermal inversion layers, by adding an unidentified optical absorber between 0.43 and 1.0 μm , with different level of opacity κ_e . The opacity of the absorber depends parabolically with frequency, with a peak value of $\kappa_e = 0.25 \text{ cm}^2 \text{ gr}^{-1}$. Two models, one with and one without an extra absorber produce similar fits to the observed z' -band flux. The best model without absorber has a $P_n = 0.3$. The best model with extra absorber has a $P_n = 0.1$ and $\kappa_e = 0.1 \text{ cm}^2 \text{ gr}^{-1}$. Observations at other wavelengths are necessary to distinguish between the three models in Figure 5.

5. DISCUSSION AND CONCLUSIONS

This first detection of the eclipse of WASP-12b confirms that the orbit of the planet is slightly eccentric, and places initial constraints to its atmospheric characteristics. The upper limits of Q'_P , obtained under the assumption that there is an additional planet in the system perturbing the orbit of WASP-12b are at least a factor of ten larger than the typically predicted value for planets of $Q'_P = 10^6$, which suggests that the planet has a core. The presence of additional planets in the system can be tested via radial velocity observations, although the current RV curve by Hebb et al. (2009) shows no evidence of additional planets, unless they are in very long orbits.

From the high levels of stellar irradiation that WASP-12b receives, one would expect that extra absorbers in its upper atmosphere do not condense out, giving rise to thermal inversion layers. However, as Figure 5 illustrates, the observed 0.9 μm eclipse depth can be fitted equally well by a model without extra absorbers. The models in the figure indicate that additional observations at wavelengths longer than $\sim 1.3 \mu\text{m}$, and prefer-

ably using narrow-band filters, are necessary to break that model degeneracy. At wavelengths shorter than 1.3 μm atmosphere models are expected to be too similar to identify differences between them with the currently achievable photometric precisions. Detections of the flux from the planet at those wavelengths should, however, still be attempted to explore the possibility that the emission of the planet short of 1.3 μm do not match the prediction of the models.

Keeping in mind that the emission of hot planetary atmospheres is unlikely to resemble a black-body, we however bring attention to the fact that the best black-body model for WASP-12b corresponds to an energy re-radiation factor of $P_n \sim 0.5$. P_n is expected to be significantly lower if the planet has a thermal inversion, but instead our result suggests that the stellar irradiation is efficiently absorbed and advected around the planet's atmosphere. However, this conclusion assumes that WASP-12b is tidally locked and with the same side always facing the star. As recently noted by Barnes et al. (2009), a close-in planet is expected to ro-

tate synchronously with the star only if it is in a circular orbit. The equilibrium rotation will be faster for slightly eccentric planets, like WASP-12b. In that case, the side of the planet facing the star varies and the stellar irradiation gets distributed over larger portions of the planetary surface, mimicking the effect of P_n . If this effect is significant, we should be observing a trend of more temperature uniform planet as orbital eccentricities increase.

M.L.M. acknowledges support from NASA through Hubble Fellowship grant HF-01210.01-A/HF-51233.01 awarded by the STScI, which is operated by the AURA, Inc. for NASA, under contract NAS5-26555. J.L.C acknowledges support from a NSF Graduate Research Fellowship. A.B. is supported in part by NASA grant NNX07AG80G. D.A. and J.C.R. are grateful for support from STScI Director's Discretionary Research Fund D0101.90131. This work has been supported by NSF's grant AST-0908278.

REFERENCES

- Anderson, D. R. et al. 2009, ArXiv e-prints
 Barnes, R. et al. 2009, ArXiv e-prints
 Bodenheimer, P. et al. 2003, ApJ, 592, 555
 Burrows, A., Budaj, J., & Hubeny, I. 2008, ApJ, 678, 1436
 Burrows, A., Hubeny, I., & Sudarsky, D. 2005, ApJ, 625, L135
 Burrows, A., Sudarsky, D., & Hubeny, I. 2006, ApJ, 650, 1140
 Deming, D. et al. 2005, Nature, 434, 740
 Désert, J. et al. 2008, A&A, 492, 585
 Fortney, J. J. et al. 2008, ApJ, 678, 1419
 Gillon, M. et al. 2007, A&A, 471, L51
 Goldreich, R. 1963, MNRAS, 126, 257
 Hebb, L. et al. 2009, ApJ, 693, 1920
 Hubeny, I., Burrows, A., & Sudarsky, D. 2003, ApJ, 594, 1011
 Ibgui, L. & Burrows, A. 2009, ApJ, 700, 1921
 Ibgui, L., Burrows, A., & Spiegel, D. S. 2009, ArXiv e-prints
 Ibgui, L., Spiegel, D. S., & Burrows, A. 2009b, ArXiv e-prints
 Kurucz, R. L. 1993, VizieR Online Data Catalog, 6039, 0
 Liu, X., Burrows, A., & Ibgui, L. 2008, ApJ, 687, 1191
 Mandel, K. & Agol, E. 2002, ApJ, 580, L171
 Miller, N., Fortney, J. J., & Jackson, B. 2009, ApJ, 702, 1413
 Pont, F., Zucker, S., & Queloz, D. 2006, MNRAS, 373, 231
 Rogers, J. C. et al., 2009, ArXiv e-prints
 Sing, D. K. & López-Morales, M. 2009, A&A, 493, L31
 Southworth, J. 2008, MNRAS, 386, 1644
 Spiegel, D. S., Silverio, K., & Burrows, A. 2009, ApJ, 699, 1487
 Sudarsky, D., Burrows, A., & Hubeny, I. 2003, ApJ, 588, 1121
 Sudarsky, D., Burrows, A., & Pinto, P. 2000, ApJ, 538, 885
 Wallenquist, Å. 1950, Arkiv for Astronomi, 1, 59
 Yoder, C. F. & Peale, S. J. 1981, Icarus, 47, 1
 Zahnle, K. et al. 2009a, AAS Meeting Abstracts, Vol. 214, 306.01
 Zahnle, K. et al. 2009b, ApJ, 701, L20